CHALMERS

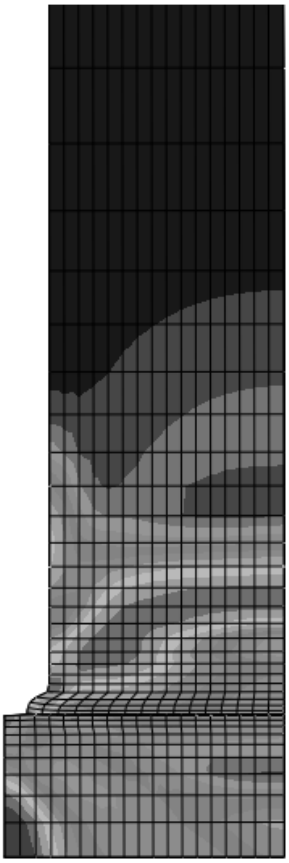

FE modeling of Orbital friction welding

Master's thesis in Applied Mechanics

IVAR WAHLSTEDT

Department of Applied Mechanics
CHALMERS UNIVERSITY OF TECHNOLOGY
Göteborg, Sweden 2016

MASTER'S THESIS IN APPLIED MECHANICS

FE modeling of Orbital friction welding

IVAR WAHLSTEDT

Department of Applied Mechanics
Division of Material and Computational Mechanics
CHALMERS UNIVERSITY OF TECHNOLOGY

Göteborg, Sweden 2016

FE modeling of Orbital friction welding
IVAR WAHLSTEDT

Master's thesis 2016:43
ISSN 1652-8557
Department of Applied Mechanics
Division of Material and Computational Mechanics
Chalmers University of Technology
SE-412 96 Göteborg
Sweden
Telephone: +46 (0)31-772 1000

Cover:
Picture of deformed mesh with stress contours

Chalmers Reproservice
Göteborg, Sweden 2016

FE modeling of Orbital friction welding
Master's thesis in Applied Mechanics
IVAR WAHLSTEDT
Department of Applied Mechanics
Division of Material and Computational Mechanics
Chalmers University of Technology

ABSTRACT

Within the European project WRIST (innovative Welding processes for new Rail InfraSTructure), an orbital friction welding (OFW) process for joining rails has been proposed. This process has potential benefits e.g. reduced heat affected zone, expulsion of impurities from the welded area and a fast welding process. To assist in the design of this welding process, finite element (FE) models will be developed within the WRIST project.

This thesis concerns the initial development of a FE model for the OFW process, applied to two bars made of a R260 rail grade. The developed FE model consists of a thermal model and a mechanical model. These are further divided into three process steps: heating, forging and cooling.

In the thermal model, two different friction models have been studied and compared against measured data from literature. Results regarding the heat generation in the faying surface (weld interface) are presented for the studied heat models. Furthermore, based on the cooling rates and a CCT-diagram for the proposed rail material, the micro-structural composition has been estimated. Results show that martensite will be created on the surface of the weld.

The mechanical model uses the temperature history from the thermal model to predict residual stresses and deformations after cooling in an sequentially coupled approach. Results from the simulation show high residual stresses. A discussion concerning the sensitivity and accuracy of predicted residual stresses and deformations, with respect to material parameters, is given.

Keywords: Heat affected zone, Orbital friction welding (OFW), residual stresses, Finite element method (FEM)

CONTENTS

1 Introduction

The thesis relates to an EU project (WRIST[1]) which aim to improve railway infrastructure; in particular the service life and quality of rail welds. One goal in the WRIST project consist of the development of two innovative welding techniques for railways [1]. These innovative techniques: *automatic forged aluminothermic welding* and *orbital friction welding* (OFW) for joining railway tracks should reduce the width of the heat affected zone (HAZ) and minimise the loss of mechanical properties around the weld. In this thesis only the OFW process is studied.

In order to develop this welding method a Finite element (FE) model that accurately portray the process is needed. A FE model is desirable since it allows fast trials of welding process parameters in computer simulations. The result from the simulations can then later be verified against measured data from experiments. This thesis focus on the initial development of a FE model for the OFW process which will provide a base for further development of a FE model for an OFW process and to provide data regarding stress fields, heat generation model and HAZ. A literature study is performed to serve as a base for knowledge about the friction welding process and to provide references for the thesis.

The report begins with an introduction and continues with the goal and limitations on the project. Then a brief description of the friction welding process and different friction welding processes. Following the introduction is a description of the material in the simulations and the geometries used in the report. Next is a description of the set up for the FE modeling, it is divided into describing the heat transfer simulation and the mechanical simulation. The report concludes with presenting the results and conclusions.

1.1 Description of the WRIST project

WRIST is a EU-project with the goal of developing and demonstrating flexible and economical ways of joining rail products. The project has partners in Universities, Rail companies and Civil-engineering companies [1]. The main goals are:

- Develop two innovative methods for welding of rails.
- Decrease fatigue damage caused by rolling contact.
- Ease maintenance and lower service costs for railways by reducing dynamic forces caused by wear in the rail surface close to the weld.
- Enable a greater use of more environmental friendly welding processes such as friction welding. This process produces no slag, fumes or smoke, which will reduce the environmental impact of track maintenance and construction.
- Provide environmental benefits by reducing emissions of carbon fuels and gas, noise, dust and vibrations from the aluminothermic process.

1.2 Purpose

The purpose is to study and develop a heat generation model for OFW of rails and to develop a FE model in ABAQUS that can be used to simulate the welding process. The modelling in ABAQUS is divided into four main parts. The first two parts is the calculation of the heat flow in two different geometries during welding. The remaining two parts is the calculation of residual stresses in the geometries after cooling. The four parts are listed below.

- **Temperature field in a square geometry during OFW**: Modelling of heat flow in OFW where the cross-section is based on a square profile. Of particular interest is the time history of the temperature field.
- **Temperature field in a rail during OFW**: Modelling of heat flow in OFW where the cross-section is based on a rail profile. Of particular interest is the time history of the temperature field.
- **Modelling of residual stresses in a square geometry during OFW**: Determine the stresses after cooling in a square geometry.

[1] Innovative **W**elding processes for new **R**ail **I**nfra**ST**ructure

- **Modelling of residual stresses in a rail during OFW**: Determine the stresses after cooling in a rail geometry.

1.3 Limitations

To save computation time, symmetries in the geometries will be used. Mesh size will be limited by the computational capacity of the computer that is used. The computers processor is a Intel core i5-2400 CPU @ 3.1 GHz with 8 GB ram. Shear forces caused by friction in the contact surface will not be modelled since the friction coefficient at high temperatures is small. Furthermore the motion of the welded objects is not simulated since moving bodies will increase the complexity of the problem.

1.4 General description of friction welding

Friction welding is a joining process where two objects are joined at high temperatures below the melting point of the material. Heat is generated in the contact surface between the welded objects due to friction caused by relative motion. When the target temperature is reached the motion stops and the objects are forged together by applying an axial force, this step is called forging. During the welding process material is expelled from the welded surface forming a flash. There exists three main types of friction welding.

- **Rotary friction welding (RFW)**: Can be subdivided into two main methods direct drive friction welding (DDFW) and inertia friction welding (IFW). In IFW a ”heavy” object is connected to one of the pieces to be joined. This object is then accelerated to a high angular velocity. Then the pieces are brought together and inertia from the heavy object sustains rotation until friction in the contact surface has dissipated enough energy. In DDFW rotation is caused by an engine that drives the process until a good weld has been achieved [2].

- **Linear friction welding**: Two pieces are brought into contact and rubbed against each other. The motion is alternating in a chosen direction. As in OFW and DDFW power is supplied externally during the process. An advantage over RFW is that non circular geometries can be joined.

- **OFW**: In OFW the pieces to be joined are moved so that the centre of the intended welding position on the stationary piece is ”orbited” by the centre of the moving piece it is then a combination of a linear and circular motion. For OFW it is found that heat is generated uniformly over the welded surface, see [3].

Some advantages of OFW worth mentioning, compared to other welds e.g. fast joining time, the welded surfaces are not in contact with oxygen which prevents oxidation, dissimilar materials can be joined and it produces a small HAZ in the components.

1.5 Behaviour of high temperature steel

The material parameters of steel is highly temperature dependent. During heating the steel transitions from a BCC (body centred cubic) structure to a FCC (face centred cubic) structure. As with water changing phase from solid to liquid there is a energy input required to drive phase transformation. To illustrate, in Figure 1.1 the specific heat is shown with respect to temperature. It can be seen that when the material undergoes a change of phase the specific heat increases. The specific heat is the energy required to increase the temperature of one kg material by one Kelvin.

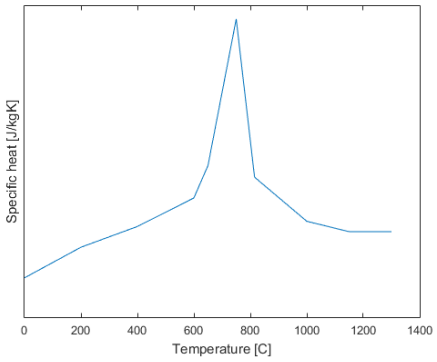

Figure 1.1: *Schematic graph of the specific heat ($\frac{J}{kgK}$) for a steel alloy.*

When steel is heated the stiffness and the yield stress also decrease. This implies that even moderate loads at high temperatures can cause significant plastic deformations in the welded material.

2 Modelling of OFW

This section describes the geometrical components that are studied in the thesis. It further presents material parameters used and modelling assumptions made. More detailed descriptions regarding boundary conditions can be found under the section boundary conditions in section 3.3.2. The material in the simulations is assumed to be homogeneous and stress free prior to welding. The ambient temperature is assumed to be 20 °C in all simulations.

2.1 Material parameters

The material data used in the model is from a WRIST data sheet [4], L. Josefsson and A. Skyttebol [5] and a paper by Balasubrahmian [6]. Most of the material data is taken from [4] for rail grade 260 steel and complemented with data from the paper when the WRIST data is not available. Kinematic hardening parameters is taken from [5].

Data is specified for Young's modulus, specific heat, thermal expansion, conductivity, density, yield strength, Poisson's ratio and hardening parameters. All the listed data given in previous list is temperature dependent and is provided as a table from which ABAQUS interpolates. For temperatures above the highest temperature given in the tables the data is set to be the value corresponding to the highest temperature in the table.

2.1.1 Kinematic hardening parameters

Kinematic hardening is added in order to improve convergence and model hardening in the material. Since material data for kinematic hardening was readily available it was added to the model. Material data for kinematic hardening is taken from the conference proceedings paper [5] page 12. At high temperatures (above 800 °C) the kinematic hardening is assumed to be linear. At low temperatures (below 600 °C) the kinematic hardening is assumed to have a value for the saturation parameter γ equal to 350 in order to set an upper limit on the hardening, a higher value will decrease the maximum stress in the simulation.

2.2 Shape of geometries in the thesis

In the thesis, two cross sections are considered: a square shaped bar and a rail. An additional part is added connecting the two pieces to be joined. This extra part (disc) is the part that is moved during welding. After welding any extra material

that is not in line with the cross-section is to be removed (only a limited amount of material is removed in the simulation). Section 2.2.1 describes the square profile and its assembly and section 2.2.2 describes the rail profile and assembly.

2.2.1 Square bar against disc

The geometry for the square bar consists of two bars and a disc. The bars and the disc are assembled as depicted in Figure 2.1a. The bars are modeled with a length of 0.3 m, this is to reduce the size of the FE model. In order to additionally decrease computational cost symmetries in the geometries is used. The geometry after dividing the square bar and disc along symmetry planes can be seen in Figure 2.1b.

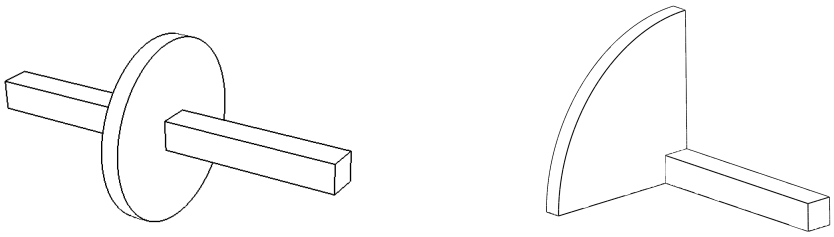

(a) *The whole Square bar geometry* (b) *Square bar with cuts along symmetry planes*

Figure 2.1: *Square bar geometries.*

The symmetries used are along the length of the bars centre axis and splitting the height of the disc in half. The total volume after symmetries are used is $\frac{1}{8}$ of the original volume.

2.2.2 Rail against disc

An UIC 60 rail profile serves as the base for the rail geometry. Pictures of the geometries before and after the split is shown in Figure 2.2. The disc has radius 0.15 m and thickness 0.030 m

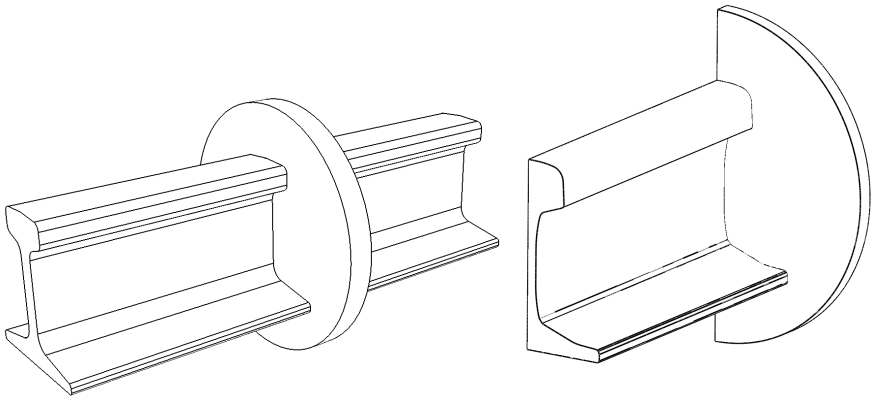

(a) *Schematic illustration of the whole rail geometry* (b) *Rail and disc split along symmetries*

Figure 2.2: *Rail geometries.*

The rail geometry is split along two symmetry planes. One along the length of the rail. The second splits the disc in half along the thickness of the disc. The volume after splits in symmetry lines is $\frac{1}{4}$ of the original volume.

3 FE modeling of OFW

From the literature study the following order of steps is proposed. Furthermore the length of heating and forging proposed corresponds to the length of the process in [3]. The length of the cooling step is set as a large time period to ensure a low temperature in the welded object at the end of the process.

- Heating 4 s
- Forging 2 s
- Cooling 1200 s

The duration of the heating step is determined by the desired temperature in the weld surface. During the heating step heat is generated in the contact surface. The heating step begins with a an increase in pressure simulating that the welded pieces is brought into contact and ends after a set time period. The forging step models the increase in pressure that forge the pieces together. No heat is generated during the forging step. In the transition from the forging step to the cooling step the contact condition in ABAQUS is changed to model bonding in the contact surface. The cooling step models the cooling of the welded area.

3.1 Modeling in ABAQUS

The calculations is split into three parts in order to decrease computational time and due to modeling constraints in ABAQUS[1]. The first part concerns the calculation of a temperature field, the second determining the stress state during heating and forging and the third part the stress response during cooling. The temperature field was calculated for the two given geometries and their surrounding area over a given time period specified as 1206 s which is the sum of the process steps. The time dependent temperature field from the heating and forging steps is imported into a mechanical analysis as a temperature field, ABAQUS then calculates the thermal stress response during the heating and forging steps. During the transition from the forging step to the cooling step, the material in the weld bond. This leads to a change in boundary conditions that needs to be modelled. In order to for ABAQUS to allow a change contact conditions, a partition in the simulation is made between forging and cooling. This partition procedure is further described in section 3.4.1. The simulation is then resumed after the split, an initial condition describing the stress state at the end of the forging phase is used as the initial state. The simulation continues until the temperature drops to levels close to room temperature.

3.2 Mesh

During meshing, effort was put into creating a mesh which had a smooth transition from the welded area to the edge of the disc. This is to capture the shape of the geometry and improve the accuracy of the results generated by the mesh [8]. Furthermore the element density is high where temperature gradients and stress gradients are presumed to be large[2] in order to further facilitate the capture of quantities of interest with large gradients. The mesh is displayed in Figure 3.1 .

The element density is greatest close to the contact surface. In order to create this mesh, partitions has been made on the geometry. These partitions split the geometry into smaller segments (cells). Smaller cells enables ABAQUS to use it's structured mesh option to generate a mesh since it divides a more complex geometry into smaller parts that have a simple geometry. Into this simple geometry a pre-meshed geometric shape can be fitted by ABAQUS. In Figure 3.2 the fitting of a mesh is illustrated. The pre meshed object to the left in Figure 3.2a is fitted to the geometry to the right 3.2(b) by moving the nodes. The overall position of the nodes and the number of node/elements are the same but the shape is different.

In Figure 3.3 the offset line, the edge of the contact area and the offset distance is shown. The offset line is the line closest to the outer edge of the disc.

The offset line is introduced to model that heat is generated on a larger surface than the contact area. The heat generating zone depends on the motion of the welded objects, if the square bar moves in a circular pattern relative to the disc, where

[1] ABAQUS can not calculate nonlinear-kinematic hardening in a coupled thermal-mechanical model [7].
[2] The area close to the weld

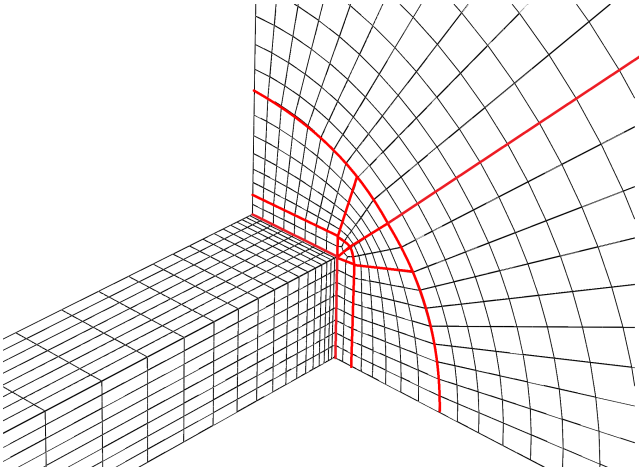

Figure 3.1: *Image of mesh for rail bar, red lines denote cell partitioning.*

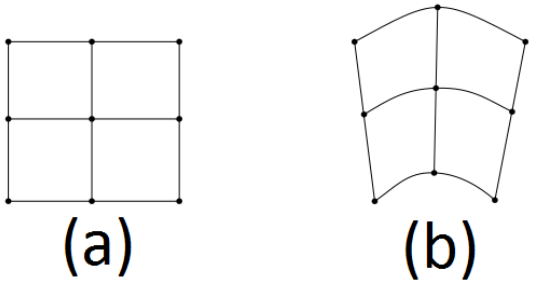

Figure 3.2: *Mapping of structured mesh.*

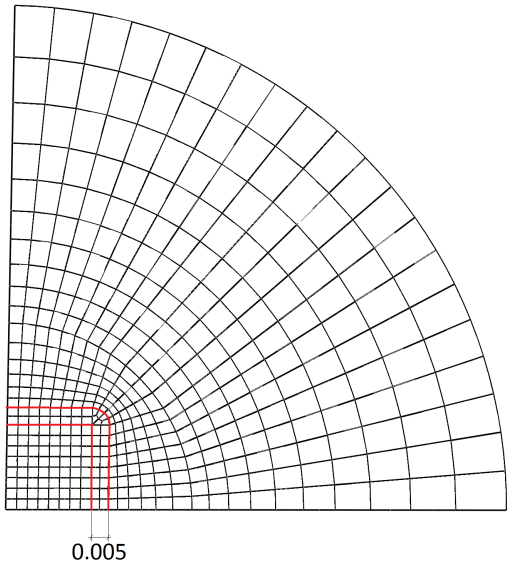

Figure 3.3: *Offset line and offset distance.*

the diameter of the circle is 0.01 m. Then the surface where the two objects is in contact at anytime is limited by a offset of 0.005 m as shown in Figure 3.4.

A mesh convergence study for the thermal mesh is performed to check if a increase in the number of elements will have an impact on the results. Data is extracted along a specified line after a simulation for two different meshes. A comparison

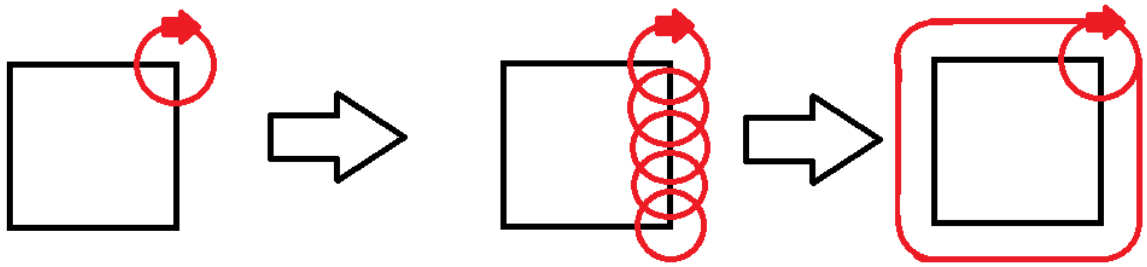

Figure 3.4: *Illustrating the offset from the square bar.*

is then made based on the difference in temperature. This is further described in section 4.1.2

The mesh for the rail is not displayed in the report due to the amount of partitions made the element size is to small to display accurately. The same procedure was applied with the same offset and settings. Due to a more complex geometry the amount of cell partitions increased.

3.3 Thermal modeling

In the Thermal model the temperature history is calculated during the whole welding process. The elements used are DC3D20 or three dimensional 20 node elements. The elements have been concentrated to the contact interface as can be seen in Figure 3.1.

The following equation is used by ABAQUS to model heat transfer 3.1. In this equation $\dot{U}$ is the material time rate of internal energy and ρ is the density, S is a surface, V is a volume, r is heat generated per volume, q describes the effect of the boundary conditions.

$$\int_V \rho \dot{U} \, \mathrm{d}V = \int_S q \, \mathrm{d}S + \int_V r \, \mathrm{d}V \tag{3.1}$$

Equation 3.1 and 3.2 is taken from [9]. The following formula describes the heat flow over the contact surface.

$$q = k(t_1 - t_2) \tag{3.2}$$

Where, t_1 is temperature for one node on one surface. t_2 is the temperature for one node on the second surface that is in contact with the first surface or ambient temperature.

Heat flow over the contact surface is specified as pressure dependent with conduction (k) values given in Table 3.1. Values for metal to air contact is given in section 3.3.2.

Pressure [MPa]	Conductance (k) $\left[\frac{W}{m^2K}\right]$
0	1e6
1e10	1e6

Table 3.1: Conductance depending on pressure for the welded surface.

Conduction values are chosen to ensure equal temperature on both sides of the contact surface. The simulation has no pressure in the interface since the heat transfer simulation can not compute pressure. This leads to that the conduction value (k) for 0 MPa is selected. In order to simplify the model heat is only added on one of the contact surfaces.

The amount of heat applied on the disk is determined by a user provided subroutine. The surface that the heat is applied to is the contact surface on the disc and an additional area outside the contact surface on the disc. This area outside the

contact surface is bounded by an offset 0.005 cm from the edge of the contact area in order to simulate that OFW motion heats a larger area around the contact. Heat is only applied during the heating step. During the forging and cooling steps no additional heat is added. The loaded area can be seen in Figure 3.3.

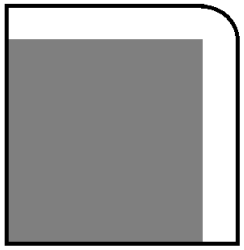

Figure 3.5: *Contact region for Square bar. The Figure describes the area in contact with the square bar (grey) and the area where heat was applied (grey and white).*

3.3.1 User provided subroutine for heat generation

The power input into the model is described by a subroutine in ABAQUS (DFLUX). Subroutines are written in FORTRAN and the subroutine is appended at the end of the report in Appendix A. The temperature dependent graph of the friction parameter is presented in Figure 3.6 together with the graph for power/area. The shape of the graph is set to resemble the friction parameter in as depicted in [3].

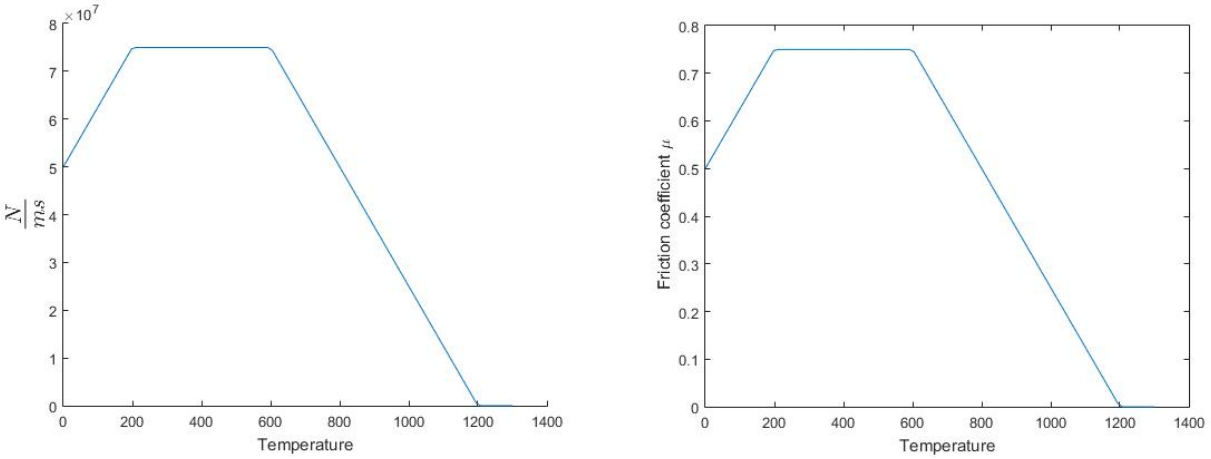

(a) $\frac{Power}{Area}$ (b) *Friction coefficient*

Figure 3.6: *Graphs for subroutine depicting the temperature dependence. The left picture describes power generated divided by area and the right the friction coefficient.*

The subroutine DFLUX calculates the heat generated based on the material state[3] in the element surfaces that lies on the loaded domain. Based on a given pressure and and velocity for the welding process the subroutine uses the temperature in the simulation to calculate the generated heat with the following formula.

$$q = \mu(T) * p * v \tag{3.3}$$

In this expression μ denotes friction coefficient, p is the pressure and v is velocity.

[3]temperature in this case

3.3.2 Boundary conditions

There are two boundary conditions in the heat transfer model in ABAQUS. The first boundary condition models the contact between steel and air, this area is called free since it is the only area that lacks a metal to metal contact, it is displayed in Figure 3.7a. The heat transmitted coefficient is set to $k_{air} = 5\ \frac{W}{m^2K}$ and the ambient temperature is set to 20 °C. The second boundary condition is the contact between the material to be welded and the welding machine's housing. This contact is a metal to metal contact. The heat transfer coefficient is set to $k_{metal} = 40\ \frac{W}{m^2K}$ and the ambient temperature is assumed to be constant 20 °C.

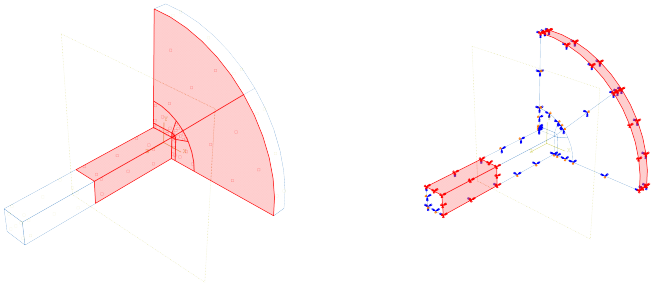

(a) *Area where boundary condition convection is applied.*

(b) *Area where boundary condition housing is applied.*

Figure 3.7: *Areas where boundary conditions is applied during the simulation.*

In the rail simulation the main difference is the change of contact area between the disc and the welded geometry. The same values are used for both boundary conditions.

3.4 Mechanical analysis

The mechanical analysis computes the stresses during the welding process. Since the material parameters is temperature dependent, the temperature history during the simulation is required. The temperature history is generated by a separate simulation over the same time span as the mechanical simulation and imported into the mechanical simulation as a thermal strain field. In this way, the effects of a thermal field can be determined from a pure mechanical analysis. In order to get the most accurate import of the thermal field the meshes should be identical with the same number of nodes in the elements. If the number of nodes in the elements differ a mapping occurs that takes time and leads to discretisation errors errors. Two runs are performed one where the disc is deformable and one where the disc is modeled as a rigid body. The rigid body model is to determine the impact of a bar to bar welding process.

The solver chosen is the dynamic implicit solver. The elements used in the mechanical simulation are linear 3D stress elements since quadratic elements are specified as unreliable for large element distortions according to the ABAQUS manual[4] [7]. Large strain formulation is used (nlgeom) since large deformations is expected in the simulation.

$$\int_V \sigma : \delta\mathbf{D}\,\mathrm{d}V = \int_S \mathbf{t}^T \cdot \delta\mathbf{v}\,\mathrm{d}S + \int_V \mathbf{f}^T \cdot \delta\mathbf{v}\,\mathrm{d}V \tag{3.4}$$

Equation 3.4 is taken from ABAQUS theory manual[10]. Where σ is the cauchy stress tensor, t is the stress on a boundary and f is the volumetric force. V denotes volume and S denotes surface. For elastic behaviour. D_{el} is a fourth-order elastic tensor and σ is a second order stress tensor and ε is a second order strain tensor.

$$\sigma = \mathbf{D_{el}} : \varepsilon \tag{3.5}$$

For plastic behaviour the yield surface (σ_0) equals.

$$\sigma_0 = f(\sigma - \alpha) = \sqrt{\frac{3}{2}(S - \alpha^{dev}) : (S - \alpha^{dev})} \tag{3.6}$$

[4] Abaqus manual 28.1.1 Solid (continuum) elements

Where S is the deviatoric stress tensor and α^{dev} is the deviatoric kinematic hardening tensor (deviatoric backstress) and α is the accumulated kinematic hardening (backstress). The model assume associated plastic flow.

$$\dot{\varepsilon}^{pl} = \frac{\partial f(\sigma - \alpha)}{\partial \sigma} \dot{\bar{\varepsilon}}^{pl} \tag{3.7}$$

Where $\dot{\varepsilon}^{pl}$ is the rate of plastic flow and $\dot{\bar{\varepsilon}}^{pl}$ equivalent plastic strain rate.

$$\dot{\bar{\varepsilon}}^{pl} = \sqrt{\frac{2}{3}\dot{\varepsilon}^{pl} : \dot{\varepsilon}^{pl}} \tag{3.8}$$

The backstress is composed of directional components where the evolution of the components are as follows.

$$\dot{\alpha}_k = C_k \dot{\bar{\varepsilon}}^{pl} \frac{1}{\sigma_0}(\sigma - \alpha) - \gamma_k \alpha_k \dot{\bar{\varepsilon}}^{pl} + \frac{1}{C_k} \alpha_k \dot{C}_k \tag{3.9}$$

Equations 3.5-3.9 are taken from Abacus user manual [11] describing kinematic hardening. Where k denotes direction, α the backstress, γ denotes saturation value (a zero value implies linear kinematic hardening), $C_k(T)$ denotes the directional temperature dependent kinematic hardening parameter and $\dot{C}_k$ is the change of the kinematic hardening parameter with time.

3.4.1 Contact formulation for mechanical simulation

The simulation of mechanical stresses in ABAQUS is split into two separate analyses in order to change the contact conditions. The split between forging and cooling is due to a model limitation in ABAQUS which do not allow changes in the contact conditions during this kind of analysis.

The first analysis step is the mechanical response during heating and forging. Here the contact is assumed to be frictionless and the surfaces are allowed to separate after contact. In the second analysis step the contact is changed to rough (no slip in contact) for the model with the deformable disc, for the model where the disc is a rigid body there is no change in contact condition. In both models the surfaces are not allowed to separate after contact. These changes should reflect the change in the contact surface when the welded material bonds as temperature decreases. The contact formulation used in the analysis' is the penalty method. In order to be able to make changes to the contact conditions between forging and cooling a restart file has to be created. This is to set the initial state for the body when starting the run in another job.

In the Mechanical response during cooling the initial state is imported by selecting predefined fields then choosing other $->$ initial state. Then select the domain that is to receive the imported data. The job name for the run we want to import from is then specified. The files has to be in the same work directory to be able to run.

3.4.2 Mesh

The mesh generated in the thermal simulation is used as a base for the mesh generation in the mechanical simulation. Due to recommendations in ABAQUS manual [7][5], the chosen element type in the mechanical simulation are three dimensional linear 8 node elements (C3D8R) with reduced integration. These contains less nodes than the three dimensional 20 node quadratic elements used in the thermal simulation which requires a mapping of the thermal field from one mesh to another. Depending on the size of the mesh this mapping process can be time consuming.

3.4.3 Loads

The load in the mechanical simulation is the pressure that forces the disc and bar into contact. It is set to vary over time as given in Figure 3.8.

The load is applied to the on the surface displayed in Figure 3.9 in the direction of the disc.

During the heating step the pressure is raised and then kept at a constant value until the forging phase. In the forging step the pressure is increased further to simulate the forging process. In the following step cooling the pressure is removed and the weld is allowed to cool.

[5] Abaqus manual 28.1.1 Solid (continuum) elements

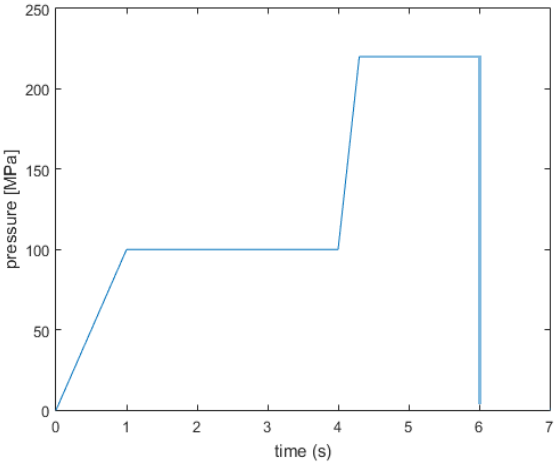

Figure 3.8: *Graph of the applied pressure.*

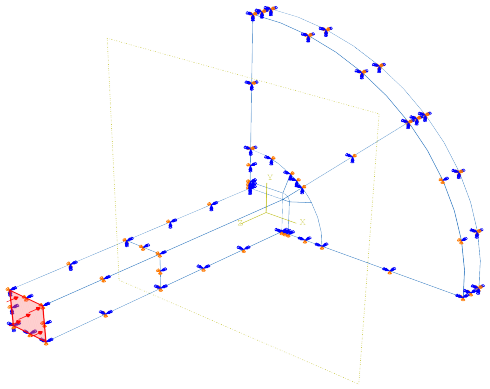

Figure 3.9: *The red area display where the pressure is applied.*

3.4.4 Boundary Conditions

The boundary conditions for the rail bar are X-symmetry, Y-Symmetry and a rigid housing that prevents movement. The housing does not add any additional stress to the model. The boundaries for the housing is specified in Figure 3.7b.

The boundary conditions for the Rail geometry are X-Symmetry and a housing that prevents movement of the disc and bar.

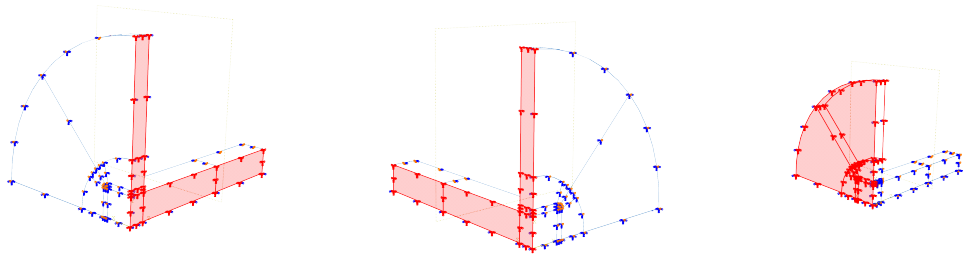

(a) *X symmetry* (b) *Y symmetry* (c) *Z symmetry*

Figure 3.10: *Boundary conditions, the shaded red areas displays the area subjected to the boundary condition.*

3.4.5 Annealing

During the Cooling step annealing is added to the model. The anneal temperature is set so that the annealed volume is the volume subjected to large deformations during the Forging step. The main reason for this is to remove the backstresses that has accumulated during the Forging from the model. The annealing material option in ABAQUS requires a ideally plastic material at and above the annealing temperature. Since the material is ideally plastic at or above the annealing temperature an applied load may cause large deformations, this leads to that no load is applied during the Cooling step instead of ramping down the load during one second in the cooling phase [12].

3.4.6 Cut

After cooling it was found that the disc causes thermal stresses by preventing the material to expand this results in that the stresses after cooling can be reduced by cutting away material. Material outside the offset line is cut away by first removing the material and adding an artificial force to keep equilibrium. This force is then reduced to zero. The stress state after this procedure is presented as the results. A Figure of the geometry after the removal of material is depicted in Figure 3.11.

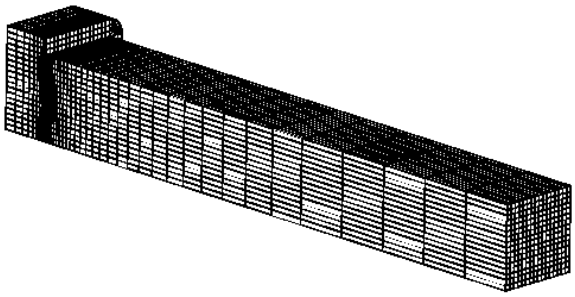

Figure 3.11: *Picture of the geometry after material is removed.*

4 Numerical studies

4.1 Validation and data extraction

Data is extracted along the following lines denoted Centre, Corner and Symmetry. When the data is plotted and the distance is displayed, the 0 value for distance corresponds to the Z symmetry plane (Figure 3.10c). When a point is named in a plot, the data for this point is taken from the the contact surface between the disc and the bar where the denoted lines intersects the contact surface. 0.015 m is the distance from the Z symmetry plane to the weld.

In the square bar geometry the lines that data is extracted along is displayed in Figure 4.1.

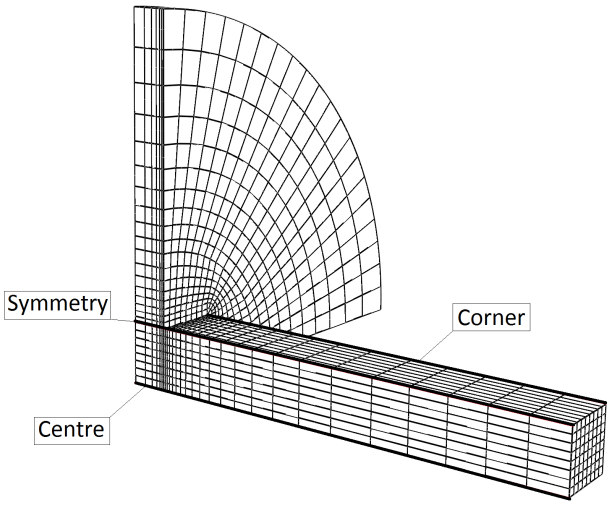

Figure 4.1: *Lines that data in plot are extracted along for a square bar.*

In the rail geometry, data is extracted from the lines displayed in Figure 4.2.

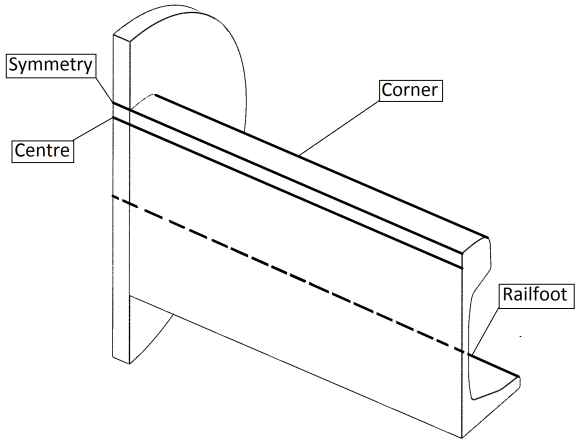

Figure 4.2: *Lines that data in plot are extracted along for a rail.*

4.1.1 Thermal validation

In order to verify the accuracy of the heat generation models, a separate thermal simulation in ABAQUS is performed. The results are compared to measured data from [6]. The thermal validation geometry consists of a square bar without disc. Both simulations is compared to the measured data and based on the result one is selected for further study. The heat input is given as described in section 3.3.1.

Heat generation validation for a square bar

Figure 4.3 and Figure 4.4 shows the calculated temperature history for the square bar at a set of nodes that lies closest to the measured points in [6]. The data in [6] is measured at a set of points. These points lie [2.54 5.08 11.43 15.24 19.05] mm from the weld interface, in the axial direction of the bar. The data extracted from the performed analysis is taken 5 mm below the surface of the square bar in the symmetry interface. In ABAQUS the time history for the nodes closest to these point was extracted and used. Figure 4.3 shows the calculated temperature history using the appended fortran code. In the literature study, a heat generation model was found that describes the friction coefficient as a function of pressure, velocity and temperature. Figure 4.4 shows the calculated temperature using the heat generation model found in literature [6]. Figure 4.5 show the measured temperature history from experiments [6].

Comparing the heat model validation graphs, it can be seen that the model in Figure 4.4 produces a peak temperature which is above the melting temperature. Because of the high peak temperature this heat generation model is not selected for further studies. The model in Figure 4.3 shows peak temperatures (close to the weld) which is of comparable size to the measured temperatures in Figure 4.5. But temperatures further from the welding surface are lower than the measured data [6]. The material used in [6] is 1045 carbon steel. Comparing material parameters in [6] to rail grade 260 steel the thermal values are of comparable size. An interval for admissible parameters (pressure, velocity and temperature) is stated in [6] and all values for the thesis simulation falls within the set boundaries. Possible sources of error for using Balasubrahmians model are: no efficiency is added in this thesis simulations, 100% of the energy produced by friction is transformed into heat[1] and expulsion of hot material to form a flash pushes cold material closer to the welded surface. This could lead to a shift in temperature where the peak temperature of 1600 °C is not reached. The [6] heat generation model describes welding of 1045 steel this may not account for the micro-structure in rail grade 260 steel. All further results are based on the procedure described in 3.3.1.

[1] some energy should dissipate in deformations

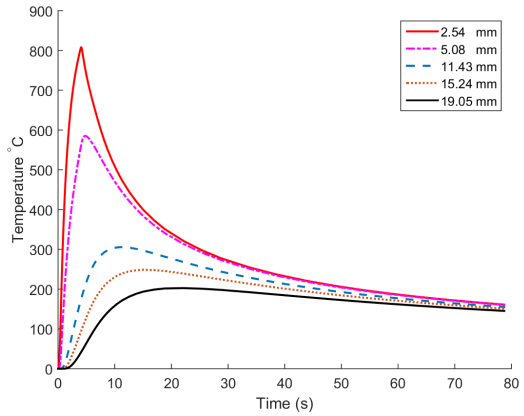

Figure 4.3: *Calculated temperature at five points for a square bar, heat is generated by the model outlined in 3.3.1.*

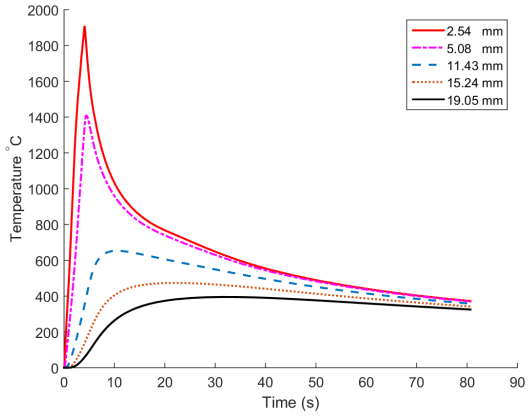

Figure 4.4: *Calculated temperature at five points for a square bar, heat is generated by Balasubrahmians friction model and calculated by fortran code in ABAQUS [6].*

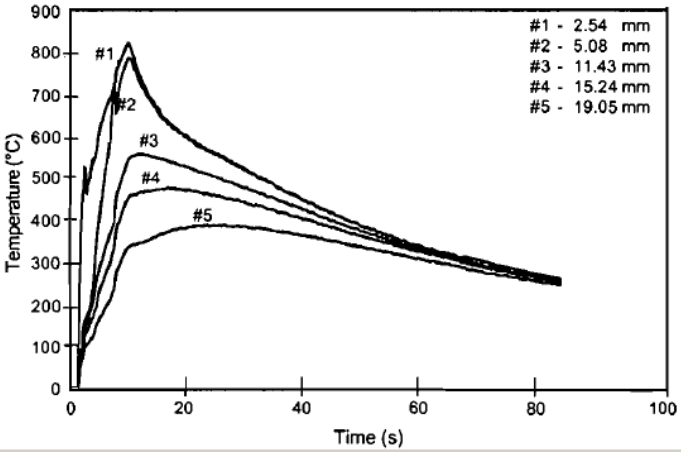

Figure 4.5: *Measured temperature at five points, from experiments [6].*

4.1.2 Thermal mesh validation

In order to verify that the mesh is able to capture the high temperature gradients that arise close to the weld interface, two different meshes are compared. These meshes differ in the amount of elements used in the simulation, the finer mesh contains roughly twice the amount of element compared to the coarse mesh. Verification is preformed by selecting a line in the computed body and comparing the temperatures for the two different meshes along this line. This procedure gave a temperature difference of 0.1 °C at the contact surface, furthermore the difference decreases when the distance to the contact are increases.

4.1.3 Maximum temperature

Maximum temperature for a square bar

The HAZ is been defined as the area where temperature rises above 700 °C at any point during the simulation. Figure 4.6 shows the maximum temperature for each point during the whole simulation. The contact surface is located at 0.015 m in the Figure (at the peak). The total width of the HAZ is here estimated to be 8 mm.

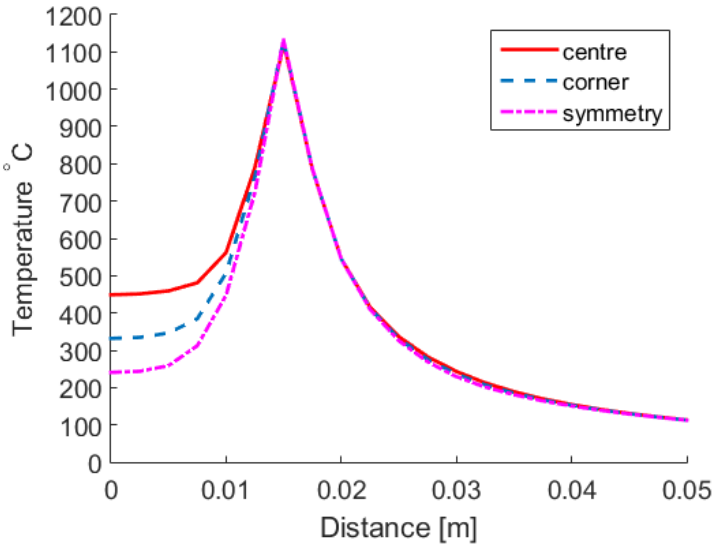

Figure 4.6: *Max temperature reached during the whole time history for specified lines in a square bar.*

Maximum temperature for a Rail

Figure 4.7 shows the maximum temperature for each point during the whole simulation. Data in Figure 4.7 is exported where the lines displayed in Figure 4.2 intersects the contact surface. The HAZ is defined as where the temperature exceeds 700 °C and is estimated to be 8 mm wide.

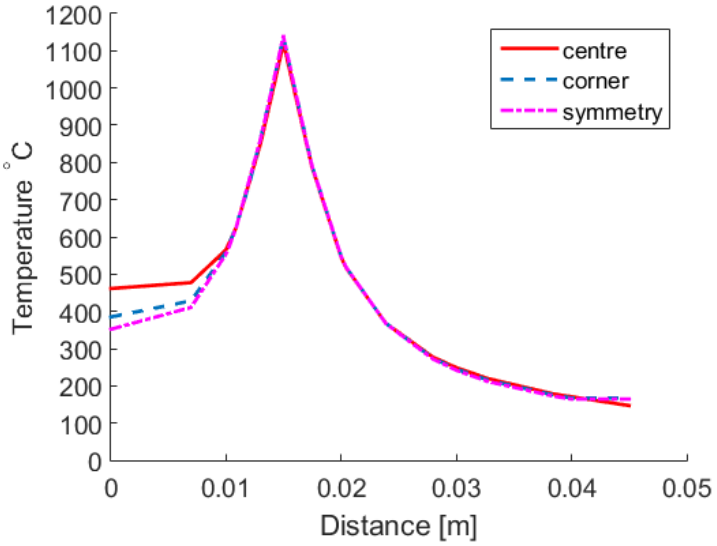

Figure 4.7: *Max temperature reached during the whole simulation for specified lines in a rail.*

The HAZ for the square bar and rail simulations is roughly of the same size (8 mm). This is larger than what is seen in from measured data from real welds [3]. However the temperature data is extracted from an undeformed model. Deformations in the contact surface should shrink the HAZ since hot material is expelled from the weld surface shortening the work piece. This expulsion occurs at the distance specified as 15 mm in Figures 4.6 and 4.7. Expulsion of material at this point brings the zones that does not exceed 700 °C during the simulation closer to each other.

Comparing the max temperature at 0 m it can be seen in Figure 4.7 that the temperature for the rail is higher than the temperature for the square bar in Figure 4.6. This is probably due to that the rail has a larger heated volume than the square bar. This leads to a larger amount of heat generated and a longer cooling time since the area that conducts heat

away does not increase as fast as the volume heated $\frac{m^3}{m^2}$.

4.1.4 CCT diagram

Continuous Cooling Transformation (CCT) diagrams show the effect cooling rate has on the micro-structure of the material. The temperature history at 3 selected points was extracted in ABAQUS and exported to a matlab script. The CCT diagram is produced with the help of JMAT-Pro version 8 [13]. The points are placed on the faying surface where the lines specified in Figures 4.1 and 4.2 intersects the contact surface. Figures 4.8 and 4.9 shows the CCT diagrams for the square bar and rail respectively.

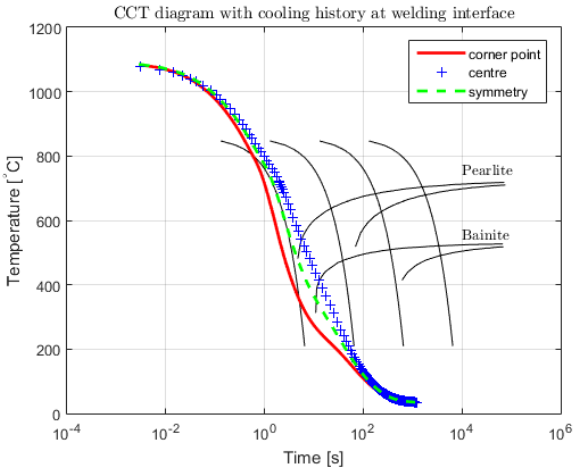

Figure 4.8: *CCT diagram for the Square bar.*

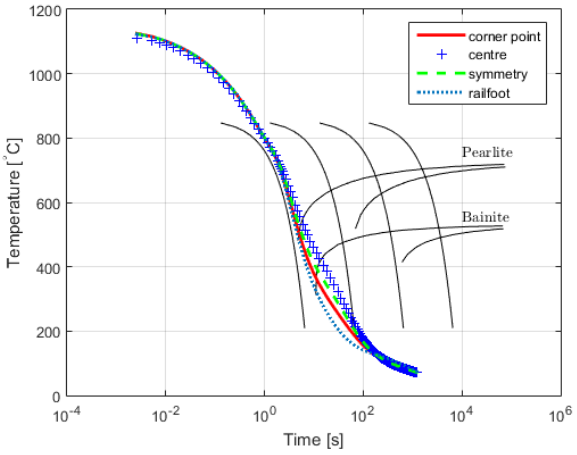

Figure 4.9: *CCT diagram for the rail geometry.*

Comparing the CCT diagrams the diagram for a square bar shows possible formation of martensite along the corner point, whereas the rail bar shows no indication of martensite formation in the corner point. The cause of this difference may be attributed to the rail edge being rounded and exposes less surface area/volume than a sharp corner. This leads to a slower cooling process. For the rail the rail-foot shows the fastest cooling rate. It however does not produce any martensite. It is assumed that the corner on the rail-foot is the area where the fastest cooling occurs.

4.2 Stress after cooling in a Square bar

The stresses in the square after cooling is extracted from the interesting lines presented earlier. Figure 4.10 displays the stress in the axial direction after cooling. Comparing the simulation with a rigid disc to the simulation where the disc is deformable the main difference can be seen in the centre. The cause of this difference is probably that since the rigid the bar is not able to expand in the axial direction and deform the rigid disc. This restriction leads to a high axial stress in the centre. Notable is that the corner and symmetry lines is under tensile stress and the centre compressive stress in the axial direction around the weld interface located at 0.015 m. The sharp dip to negative values are located at the tip of an inverse corner possibly acting as a notch which focuses stress here. The cause of the notch is rapid change in temperature over an element during loading combined with a rapid change of stiffness depending on temperature in the material. This results in that the top of the element is stiff and the bottom is soft leading to a large displacement in the element. Comparing the maximum stress in the z-direction presented in Figure 4.10 to results presented in [5] it can be seen that the maximum stress in the z-direction presented in this thesis is lower than the maximum stress in [5].

Figure 4.11 displays the Von Mises stress for three lines after cooling. Comparing the simulations the largest difference between the rigid body simulation and the deformable simulation occur near the weld interface in the centre and corner.

The shear stress in the plane parallel to the disc is displayed in Figure 4.12. The largest shear stresses occur in the corner of the square bar. Note that the shear stress in the corner has the same shape in the interval 0.015 m to 0.022 m.

Comparing the deformations obtained from the simulation presented above (deformations shown i Figure 4.14) to deformations in literature [3] the obtained in this thesis are small. To check if shear locking occurs in the simulation the

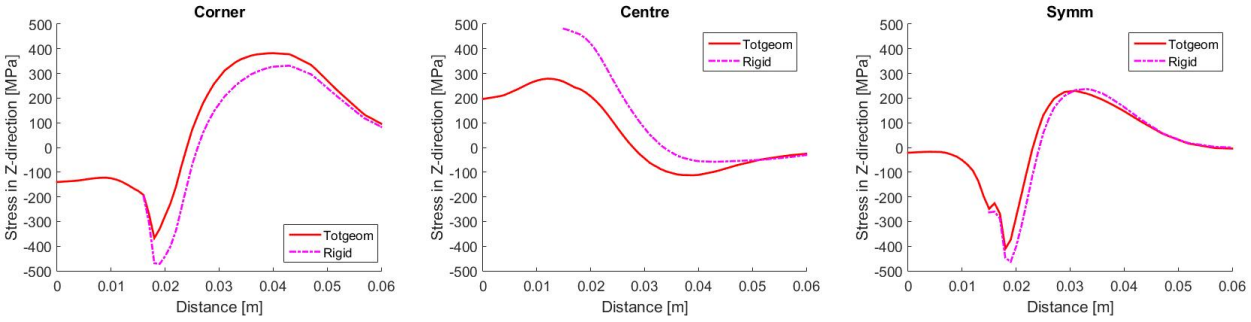

(a) (b) (c)

Figure 4.10: *Axial stress for square bar.*

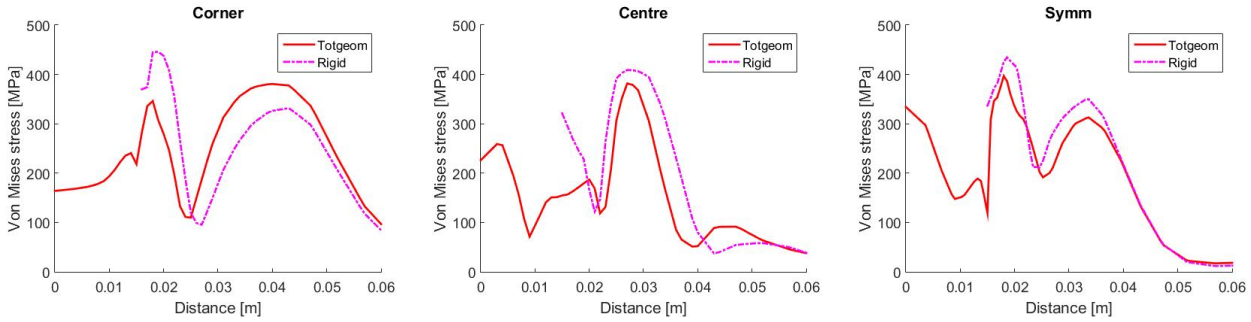

(a) (b) (c)

Figure 4.11: *Von Mises stress.*

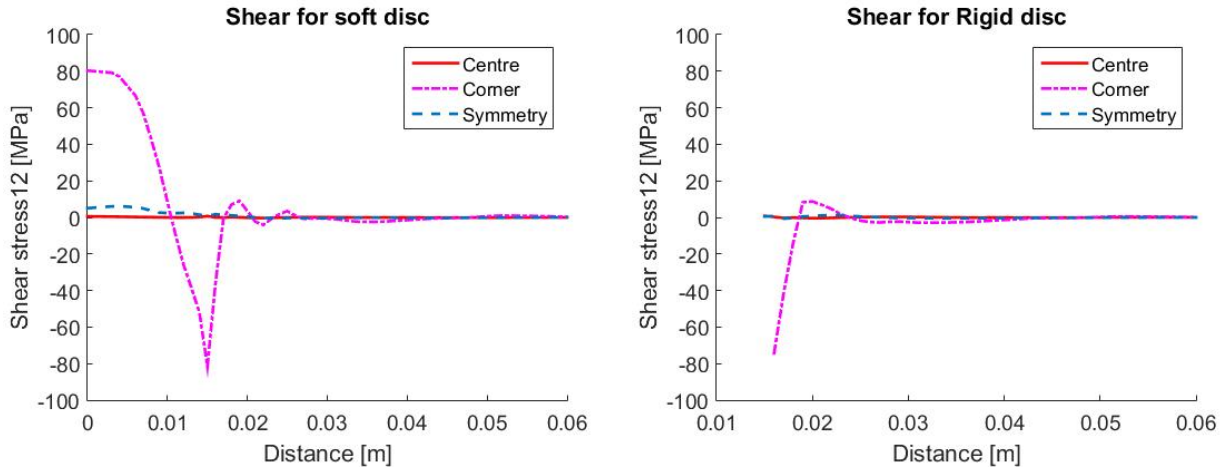

(a) (b)

Figure 4.12: *Plot of the shear stress perpendicular to the axial direction of the square bar.*

element size near the interface was decreased this was found to have no effect. After the decrease in element size the effect of decreasing the yield stress above 700 °C was investigated, this resulted in larger deformations. The deformations for lower yield stress is shown in Figure 4.13 as well as the deformation for the model that the results presented is extracted from. This indicates that the current amount of data points describing the material above 700 °C is to few. Currently the data for yield stress is given at four points at 20 °C, 650 °C, 800 °C and 1300 °C. In order to improve the accuracy of the results more data points for high temperatures (above 700 °C) is needed.

One possible source of error is that no convergence study for the mechanical simulation was performed. The result may change with an increase in mesh refinement. This is especially important in the area around the weld where large temperature gradients occur. Also since the simulation is a sequentially coupled simulation where a calculated temperature

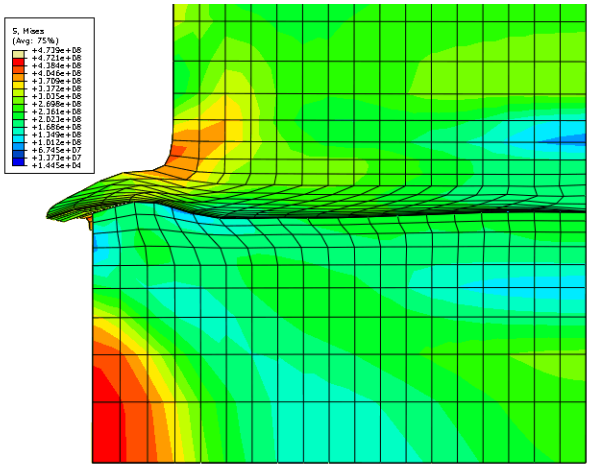

Figure 4.13: *Lowered yield stress.*

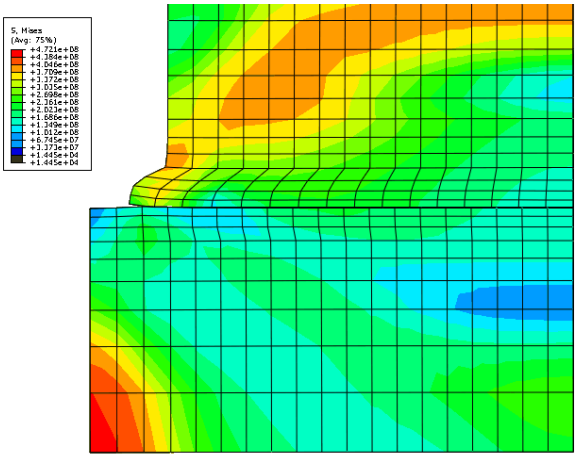

Figure 4.14: *Yield stress before changes.*

field is imported into a mechanical simulation, the deformations cause no further heating of the area around the weld. This is somewhat inaccurate as shown in [2] energy generated by plastic work contributes to the heating of the welded object. However compared to the heat generated by friction this additional energy input caused by deformations is small, thus it is neglected in this thesis. For further work the effect on the temperature field by plastic deformation would be interesting. But more pressing matters would be that the sequentially coupled simulation inaccurately simulate the temperature in surface areas in the welded zone that begin in contact and after some deformation are no longer in contact. Since the temperature field is previously calculated and imported into the mechanical simulation this area will still generate heat by friction even-though it is not in contact with another surface. This happens because the heat transfer simulation has no deformations thus it cannot account for deformations occurring in the mechanical simulation since the mechanical simulation is performed after the thermal simulation. This mismatch in the temperature field is probably greater that the added heat by deformations. A possible solutions is to perform the simulation as in this thesis then export the time dependent deformations to a new heat transfer simulation that is then used for a new mechanical simulation.

Material data for high temperatures consists of a few data points above 700 °C. Since the simulation is temperature dependent more data points may lead to a improved result. In particular the saturation parameter γ has a large effect on the maximum stress reached during cooling since it limits the amount of kinematic hardening in the model. A increase in γ will lead to lower stresses in the simulation. Since no data for the size of this parameter exists for the material used a value has been assumed. This value may be to low or to high.

Change in geometry

Geometry improvements include the removal of some material as shown in Figure 4.15. The reason for removal of material is that temperature in the centre of the disc close to the bar is hot and the outer edge of the disc is cool. This difference in temperature means that the thermal expansion in the centre is limited in the radial direction by the cool side of the disc. This causes stresses during the cooling phase. The proposed change in the disc's geometry may decrease the stress in the weld interface after cooling.

4.3 Stresses in rail geometry after cooling

No results for cooling in the rail is available. Using the same settings as for the square bar the simulation took to much space on the hard drive and time to complete. Thus only data for the stresses for the square bar is presented.

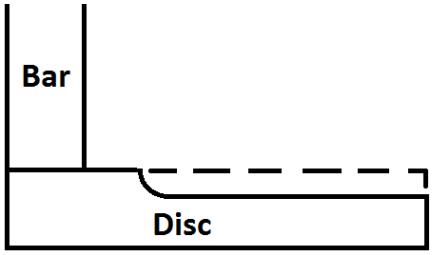

Figure 4.15: *Image of new geometry.*

5 Conclusion

In this thesis, a FE model of a new orbital friction welding process has been developed and then used to study welding of bars and rails. The developed model included three simulation steps: heating, forging and cooling. The process has been modeled using a sequentially coupled analysis where the temperature field from a heat transfer analysis has been imported into a mechanical analysis.

Results from the heat transfer simulations show that the calculated temperature field reported in roughly corresponds to the measured temperature field literature for a steel bar (without disc). This indicates that the chosen heat generation model produces an adequate approximation of the heat generated during the welding process.

Cooling rates are determined from the simulated temperature history, and visualised in CCT diagrams, indicates possible martensite formation in the corners of the square bar. However in the case of welding of a rail profile, no martensite formation can be seen in either disc or rail. This indicates that orbital friction welding of rails may be a viable welding procedure.

The residual stress state, after cooling and removal of excess disc material, has been simulated. It was found that the stress magnitude was reduced by the removal of material around the weld by comparing an uncut geometry to a geometry where material was removed. The obtained residual stresses, in the longitudinal direction, were seen to be somewhat lower than that presented in [5]. This may be attributed to the difference in welding method used and difference in material parameters.

Since the simulation is sequentially coupled there are inaccuracies regarding the temperature field in the mechanical simulation since the contact region in the heat transfer simulation does not represent the contact region in the mechanical simulation where deformations occur. This implies a need for a coupled simulation to increase the accuracy of the temperature history. Other sources of errors includes the omission of a mesh convergence study for the mechanical response.

Due to time constraints, residual stresses were only obtained for the bar cross section; therefore, future work includes determining the residual stress state also for the rail. The residual stresses are very dependent on the mechanical behaviour of the rail material but unfortunately there is large uncertainty in the material behaviour, especially at elevated temperatures. Therefor, additional work in determining accurate material data is of high importance.

References

[1] *WRIST-project Webpage*. http://www.wrist-project.eu/page/en/about-wrist/objectives-and-targeted-results.php. Accessed: 2016-06-10.

[2] D. Schmicker, K. Naumenko, and J. Strackeljan. A robust simulation of Direct Drive Friction Welding with a modified Carreau fluid constitutive model. *Computer Methods in Applied Mechanics and Engineering* **265** (2013), 186–194.

[3] M. Maalekian. Grandjon prize competition 2008 Joint Winner – Category A: "Joining and Fabrication Technology" characterization and optimization of orbital friction welding of high carbon steel bars. *Welding in the world* **53** (2009), R109–R123.

[4] J. Brouzoulis and L. Josefsson. *WRIST internal report WP4*. 2015.

[5] *Numerical simulation of flash butt-welding of railway rails Proceedings from the 7th International Seminar on Numerical Analysis of Weldability*. GrazSeggau (Austria), 2003, 21 pp.

[6] V. Balasubramanian et al. A New Friction Law for the Modelling of Continuous Drive Friction Welding: Applications to 1045 Steel Welds. *Materials and Manufacturing Processes* **14**.6 (1999), 845–860.

[7] Dassault-systems, ed. *Abaqus 6.14, Analysis User's Guide; 23.2.2 Models for metals subjected to cyclic loading*.

[8] V. Adams. *A designer's guide to simulation with finite element analysis*. Ed. by NAFEMS. 2008. ISBN: 978-1-874376-32-3.

[9] Dassault-systems, ed. *Abaqus 6.14, Theory Guide; 2.11.1 Uncoupled heat analysis*.

[10] Dassault-systems, ed. *Abaqus 6.14, Theory Guide 2.1.1 Procedures: overview and basic equations*.

[11] Dassault-systems, ed. *Abaqus 6.14, Theory Guide; 4.3.5 Models for metals subjected to cyclic loading*.

[12] Dassault-systems, ed. *Abaqus 6.14, Analysis User's Guide; 23.2.5 Annealing or melting*.

[13] *JmatPro Webpage*. http://www.sentesoftware.co.uk/jmatpro.aspx. Accessed: 2016-09-07.

A FORTRAN

```
SUBROUTINE DFLUX(FLUX,SOL,KSTEP,KINC,TIME,NOEL,NPT,COORDS,JLTYP,
1 TEMP,PRESS,SNAME)
INCLUDE 'ABA_PARAM.INC'
DIMENSION FLUX(2), TIME(2), COORDS(3)
REAL*8 MU, MUP, MU0, P, P0, V
CHARACTER*80 SNAME
P0 = 100000000.0D0
V = 1.0D0
MU0 = 0.5D0


P = -1.0D0
if (TIME(2) .LT. 1.0D0) then
P = P0*TIME(2)/1.0D0
else
P = P0
endif



MU = -1.0D0
if (SOL .LT. 200.0D0) then
MU = MU0*(1.0D0+0.5D0*SOL/200.0D0)
MUP = MU0*(0.5D0*SOL/200.0D0)

elseif (SOL .LT. 600.0D0) then
MU = 1.5D0*MU0
MUP = 0.0D0

elseif (SOL .LT. 1200.0D0) then
MU = 1.5D0*MU0-(1.5D0*MU0/(1200.0D0-600.0D0))*(SOL-600.0D0)
MUP = -(1.5D0*MU0/(1200.0D0-600.0D0))*SOL
else
MU = 0.0D0
MUP = 0.0D0
endif


FLUX(1) = MU*P*V
FLUX(2) = 0.0D0



RETURN
END
```